

Time-modulated convection with zero mean temperature gradient

A. C. Or and R. E. Kelly

Department of Mechanical and Aerospace Engineering, University of California at Los Angeles, Los Angeles, California 90095-1597

(Received 8 January 1999)

We study numerically the onset of temporally modulated Rayleigh-Bénard convection with zero mean gradient for cases of antisymmetric and asymmetric boundary temperatures over a continuous range of non-dimensional frequencies ω , from $\omega \sim O(10^{-1})$ to $\omega \sim O(10^3)$. For ω below 1, the neutral curves for $Pr=7$ in both cases alternate between synchronous and subharmonic responses, with increasingly shorter intervals as ω becomes small. At large ω , the critical wave number k_c asymptotes to $\omega^{1/2}$ and the critical Rayleigh number R_c asymptotes to $\omega^{3/2}$, via a subharmonic response in both cases. A comparison with the experimental results of Niemela and Donnelly [Phys. Rev. Lett. **57**, 583 (1986)] shows fairly reasonable agreement. [S1063-651X(99)08608-0]

PACS number(s): 47.20.Bp

I. INTRODUCTION

Many investigations have been aimed at determining how periodic modulation with time of the temperature of one or both of the horizontal walls affects the onset of Rayleigh-Bénard convection; for a report of experimental results for heating at the lower wall and a survey of theoretical analyses, see the paper by Meyer *et al.* [1]. An interesting limit of this problem concerns the case when the modulation amplitude is very large in comparison to the characteristic temperature difference of the mean state and when the characteristic diffusion length associated with the modulation, i.e., $(\omega^*/2\kappa)^{-1/2}$, where ω^* is the dimensional frequency and κ is the thermal diffusivity, is small in comparison to the thickness, d , of the fluid layer. When these conditions are fulfilled, the linear problem reduces to determining the stability of a thermal Stokes layer with zero mean gradient. This limit of the general problem was studied first by Gershuni and Zukhovitskii [2] (see also Sec. 36 of the book by these authors [3]) by means of a severely truncated Fourier expansion. Nonetheless, their theoretical result compares reasonably well with the more recent experimental results of Niemela and Donnelly [4]. In particular, a subharmonic disturbance was observed to be most critical. The same numerical approach was used for the nonlinear problem by Swift and Hohenberg [5], except that they allowed for the generation of a mean temperature field. They found that a subcritical bifurcation is possible, which was evident in the experiment of Niemela and Donnelly [4] via the occurrence of hysteresis.

When $(\omega^*/2\kappa)^{-1/2}$ is comparable to d , the approximate results of Gershuni and Zukhovitskii [3] and the more accurate results of Yih and Li [6] exist for the case of zero mean temperature gradient. The former results at best are restricted to very low nondimensional frequencies because the temperature gradient is taken to be independent of distance normal to the wall. Although the numerical results of Yih and Li are not restricted by this assumption, the accuracy of their results is restricted somewhat by the fact that only two terms were used in their spectral expansions. However, the results of both research groups agree in the prediction that alternating regions of synchronous and subharmonic critical modes

exist as the frequency varies (this kind of behavior has been found more recently by Kumar [7] for the case of Faraday waves on the surface of a viscous layer of liquid; see also Cerda and Tirapegui [8,9]).

It is not obvious how the solution regime existing for nondimensional frequency $\omega = (\omega^* d^2 / 2\kappa)$ of $O(1)$ changes as ω increases so as to permit only a subharmonic solution rather than further alternating solutions. The present calculations have been done mainly to fill in this gap. However, in the process, more accurate, fully converged results in general have naturally been obtained and are presented.

II. MATHEMATICAL FORMULATION

We consider an infinite horizontal layer of an incompressible fluid of thickness d . The layer is bounded above and below by rigid walls. The layer is isothermal at a temperature T_0^* in the absence of modulation. Then we impose a sinusoidal temperature $T_\delta^* \cos \omega^* t^*$ (asterisk denotes dimensional quantities) on the lower wall. We scale length, time, velocity, pressure relative to the hydrostatic reference value, and temperature relative to T_0^* by d , ω^*^{-1} , κ/d , $\rho\nu\kappa/d^2$, and T_δ^* , respectively. The governing nondimensional equations are as follows:

$$2\omega Pr^{-1} \partial_t \mathbf{U} + \mathbf{U} \cdot \nabla \mathbf{U} = -\nabla P + \nabla^2 \mathbf{U} - R T \mathbf{k}, \quad (1)$$

$$\nabla \cdot \mathbf{U} = 0, \quad (2)$$

and

$$2\omega \partial_t T + \mathbf{U} \cdot \nabla T = \nabla^2 T, \quad (3)$$

where \mathbf{k} denotes the vertical downward direction so that the upper and lower walls are located at $z=0$ and 1, respectively. The nondimensional frequency is given by $\omega = \omega^* d^2 / 2\kappa$, the Prandtl number by $Pr = \nu / \kappa$, and the Rayleigh number by $R = \alpha g T_\delta^* d^3 / \kappa \nu$, so that R depends on the amplitude of the modulation. The basic state is one of no motion, with $\mathbf{U} = \mathbf{0}$, and a nondimensional basic temperature, $T(z, t)$, defined by the relationship $T^*(z, t) = T_0^* + T_\delta^* T(z, t)$. To compute $T(z, t)$, we consider in turn two

situations. The first case corresponds to an asymmetric modulation of the basic temperature. In this case, we impose at the lower wall the following boundary condition:

$$T(1,t) = \cos t, \quad (4a)$$

while the upper boundary is assumed to be perfectly conductive so that

$$T(0,t) = 0. \quad (4b)$$

In the case of Niemela and Donnelly [4], the modulation is prescribed on the upper wall but there is no mention about the thermal boundary condition at the lower wall. In Swift and Hohenberg [5], the modulation is on the lower wall while a thermal boundary condition of the mixed type is applied at the upper wall. Our perfectly conductive upper wall corresponds to $\lambda_w = \infty$ in the upper-wall thermal condition given by their equation (2.5), whereas Swift and Hohenberg used a value $\lambda_w = 0.27$ in order to compare with experimental results.

The second case we consider corresponds to an antisymmetric modulation of the basic temperature. We then impose at the upper wall the following boundary condition:

$$T(0,t) = \cos t, \quad (5a)$$

and at the lower boundary

$$T(1,t) = -\cos t, \quad (5b)$$

which are the same boundary conditions used in Yih and Li [6]. The governing equation is

$$2\omega T_t = T_{zz}. \quad (6)$$

The solution $T(z,t)$ to the asymmetric problem from Eqs. (4a), (4b) and (6) is

$$T(z,t) = \frac{1}{2} \left\{ \frac{\sinh(i\omega)^{1/2} z}{\sinh(i\omega)^{1/2}} e^{it} + \text{c.c.} \right\}, \quad (7a)$$

where ‘‘c.c.’’ denotes the complex conjugate. Similarly, the solution $T(z,t)$ to the antisymmetric problem from Eqs. (5a), (5b), and (6) is

$$T(z,t) = \frac{1}{2} \left\{ \frac{\sinh(i\omega)^{1/2} (1/2 - z)}{\sinh((i\omega)^{1/2}/2)} e^{it} + \text{c.c.} \right\}. \quad (7b)$$

We now superimpose a perturbation temperature $\theta(x,y,z,t)$ on T and introduce the corresponding perturbation velocity components u, v, w and pressure p . After eliminating the pressure and horizontal velocities, we obtain the following perturbation equations:

$$2\omega \text{Pr}^{-1} \nabla^2 w_t - \nabla^4 w = -R \nabla_{\perp}^2 \theta, \quad (8)$$

and

$$2\omega \theta_t - \nabla^2 \theta = -T_z(z,t) w. \quad (9)$$

The horizontal Laplacian ∇_{\perp}^2 is defined as $(\partial_{xx} + \partial_{yy})$. For the perturbations w and θ , symmetric rigid and isothermal boundary conditions are imposed at $z=0$ and 1, giving

$$w(0) = \theta(0) = w(1) = \theta(1) = 0. \quad (10)$$

Because of the horizontal isotropy of the layer, it is sufficient to look for two-dimensional solutions of the following form:

$$(w, \theta) = (W(z,t), \Theta(z,t)) e^{ikx} + \text{c.c.} \quad (11)$$

The numerical method used for solving the above problem is standard (see, for example, Or [10]). We first expand the z dependence of the variables using the Chebyshev functions, as follows:

$$W(z,t) = \sum_{n=0}^{N_t} a_n(t) T_n(x), \quad \Theta(z,t) = \sum_{n=0}^{N_t} b_n(t) T_n(x), \quad (12)$$

where N_t is a truncation number and x exists in $[-1,1]$ and can be transformed to the physical domain $[0,1]$ by $z = (x+1)/2$. Upon the substitution from Eqs. (11) and (12) into the governing equations (8) and (9) and utilizing the boundary conditions (10) (using the Tau method), we obtain a finite matrix equation of the following form:

$$2\omega \mathbf{B} \dot{\mathbf{x}} = \mathbf{A} \mathbf{x} + i \mathbf{F}(t) \mathbf{x}, \quad (13)$$

where all the matrices are real; \mathbf{B} and \mathbf{A} are time-independent and $\mathbf{F}(t)$ is 2π -periodic. The state vector \mathbf{x} consists of an arrangement of the Chebyshev coefficients $a_n(t)$ and $b_n(t)$ (for $0 \leq n \leq N_t$). We then apply Floquet theory to expand the vector-dependent variable in the form of Fourier series. The general response of $\mathbf{x}(t)$, for example; is given by

$$\mathbf{x}(t) = \sum_{m=-N_p}^{N_p} \mathbf{x}_m e^{(im + \sigma)t}, \quad (14)$$

where the \mathbf{x} ($-N_p \leq m \leq N_p$ for a truncation number N_p) is a set of constant vector Fourier coefficients and σ is in general a complex Floquet exponent. We look for synchronous and subharmonic solutions separately using an iteration approach, corresponding to $\sigma_i = 0$ and $\frac{1}{2}$, respectively. We have also considered more general values of σ_i but so far no unstable quasiperiodic solution has been found. The convection occurs in the form of either synchronous or subharmonic modes, as will be described in the next section.

III. NUMERICAL RESULTS

We first present results for the asymmetric case. This case is studied more extensively here in order to compare with the experimental results [4]. Then we present some results on the antisymmetric case, which serve as an extension of Yih and Li's results [6].

A. Asymmetric case

First, we consider a fluid with $\text{Pr}=7$. Results for other values of Pr will be given later. For this case, numerical convergence is good at large ω at which we use 14 Chebyshev modes in z and 24 Fourier modes in t as representations. At lower ω , convergence becomes slower in terms of the number of iterations required as well as larger N_t and N_p required for convergence. As discussed by Barenghi and Jones [11] and others, the use of Floquet theory to describe

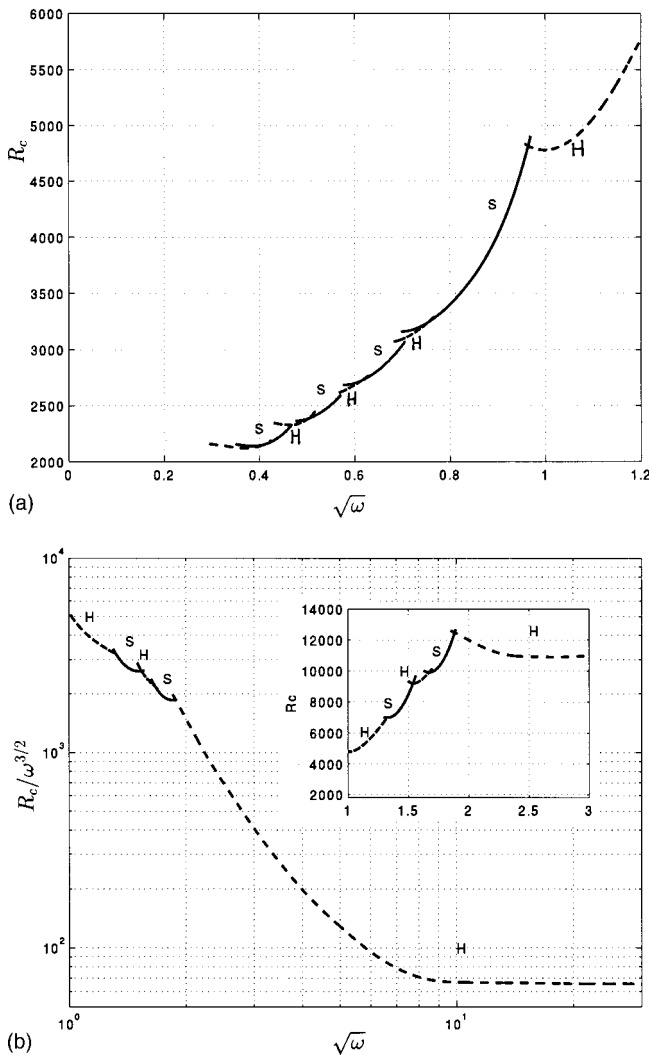


FIG. 1. (a) A low-frequency plot of R_c vs $\omega^{1/2}$ for the case of an asymmetric basic temperature with $Pr=7$; (b) a higher frequency log-log plot of $R_c/\omega^{3/2}$ vs $\omega^{1/2}$. The inset to (b) shows the same curves without the asymptotic scaling to emphasize the alternating characteristics of the curves.

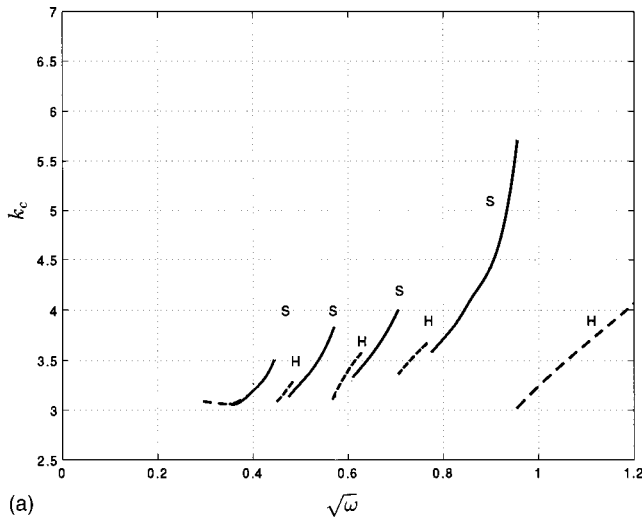
the stability of the system becomes questionable for low ω . Nevertheless, in this case we compute results down to $\omega = 0.09$.

Figures 1(a) and 1(b) show plots of critical-curve dependence on frequency. Due to the large range of frequency scale, we divide the stability curves into two parts. Figure 1(a) shows the lower-frequency and Fig. 1(b) shows the higher-frequency range. The log-log scale in Fig. 1(b) appears more suitable for the purpose of presentation of the high-frequency range in order to demonstrate the asymptotic limit of the thermal Stokes layer as $\omega \rightarrow \infty$. However, for clarity we also include the more customary plot of the same curves in the inset. For ω smaller than 1, Fig. 1(a) reveals an alternating pattern of S and H modes. As ω becomes smaller, the critical curves appear to decrease in width. At low frequency a larger number of base functions is needed to achieve numerical convergence of the solutions. For example, at $\sqrt{\omega}=0.3$, both N_t and N_p have to be 80% larger than those corresponding values at $\sqrt{\omega}=1$. Computing the critical curves becomes increasingly difficult below $\sqrt{\omega}$

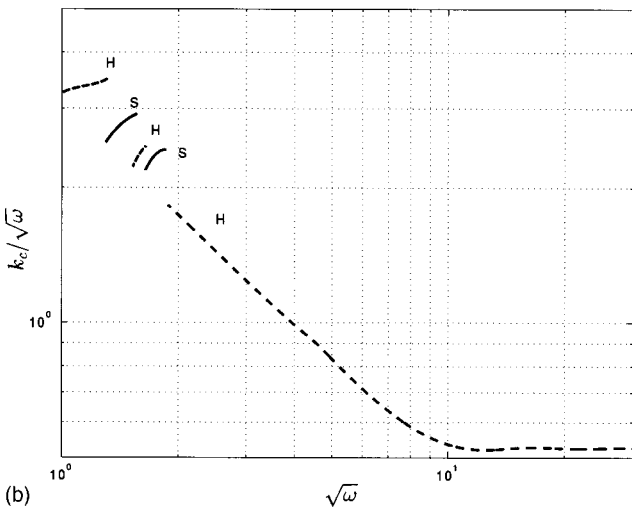
$= 0.3$. Therefore, we cut off the plot at $\sqrt{\omega}=0.3$.

The appearance of increasingly closely spaced loops while taking the limit $\omega \rightarrow 0$ is a behavior reported by Cerda and Tirapegui [8,9] and Dowden [12]. These two studies concern, respectively, an isothermal layer with a free surface undergoing low-frequency gravitational modulation and the problem of Rayleigh-Bénard convection with free-slip boundary conditions. The difference between Dowden's and Cerda and Tirapegui's results, however, is the absence of the subharmonic loops in the case of Dowden's result (see Fig. 1 of [12]). The alternating stable regions in the case of Dowden are filled by the unstable loops of subharmonic solutions in our case and in the case of [8,9].

In the inserted panel in Fig. 1(b), we reveal the structure more clearly by plotting R_c . The striking feature shown there of alternating synchronous (S) and subharmonic (H) critical curves was also observed earlier for the antisymmetric case by Yih and Li [6] (we also use their abbreviations for the two modes). While previous results have either explored the $\omega^{1/2} \sim O(1)$ region or the region for asymptotically large ω , Figs. 1(a) and 1(b) together give a display of the critical curves for a wide-continuous range of frequency. Figure 1(b) shows that the alternating pattern ceases when $\omega^{1/2} \approx 1.9$, which is a new result. Beyond this value, instability is dictated solely by a subharmonic response. Furthermore, the quantity $R_c/\omega^{3/2}$ asymptotes to a constant value, corresponding to $R_c \approx 65.5\omega^{3/2}$ when $\omega^{1/2} > 10$, indicating the onset of an asymptotic balance. In Figs. 2(a) and 2(b), respectively, we show a regular and a log-log plot for k_c and $k_c/\omega^{1/2}$ versus $\omega^{1/2}$. These critical wave-number curves correspond to the critical curves of Figs. 1(a) and 1(b). For $\omega^{1/2} \sim O(1)$, the critical wave number becomes discontinuous at intersections between the synchronous and subharmonic neutral curves. The various k_c associated with the neutral-curve loops appear as the slanted curves bounded approximately between values 2 and 5. Figure 2(b) shows that there is a characteristic change for the last k_c curve corresponding to the asymptotic subharmonic mode. This last k_c curve tilts in an opposite sense to that of the other curves. The asymptotic relationship is $k_c \sim 0.525\omega^{1/2}$, approximately. The alternating structure between S and H modes for moderate ω does not seem to have a simple explanation. We examined the magnitude of $|\mathbf{x}_m|^2$ of each harmonic mode and found that the fundamental mode ($m=1$) is always the dominant mode. Thus, it is unlikely that the individual critical curves are due to different higher harmonics that become unstable. We note that Cerda and Tirapegui [8] interpret the alternating structure that they found at low frequency for an isothermal layer undergoing gravitational modulation as indicating the appearance of an additional mechanism for instability, namely, Rayleigh-Taylor instability in addition to the usual mechanism of parametric resonance. In [9], the authors present the results in significantly greater detail. Here, the sign of basic temperature gradient is analogous to the sign of vertical acceleration in the case of [8,9]. The physical instability mechanisms for the two situations differ, but the bifurcation structures are sufficiently similar in the low-frequency range that a broader view of the modulated instability is appropriate. Since the asymptotic limit $\omega \rightarrow 0$ cannot be approached by direct numerical computations, in a separate note [13],



(a)



(b)

FIG. 2. (a) Corresponding plot of k_c vs $\omega^{1/2}$, and (b) corresponding log-log plot of $k_c/\omega^{1/2}$ vs $\omega^{1/2}$ for the asymmetric case.

this limit will be analyzed by the WKB approach to bridge the gap.

Results at other values of the Prandtl number are available from the previous work of Gershuni and Zhukhovitskii [3] and Niemela and Donnelly [4]. We extend our results to lower Prandtl numbers in order to make comparisons possible. We first compute the critical Rayleigh number versus Pr for two cases of frequency: (i) $\omega^{1/2}=30$ and (ii) $\omega \rightarrow \infty$. In case (ii) the problem is computed on a semi-infinite domain [3]. The Chebyshev base functions are still used, but the x domain $[-1, 1]$ for this set of functions is mapped to the ξ domain $[0, \infty]$ by using an algebraic transformation [14] $\xi = L(1+x)/(1-x)$, where L is a length scale of the mapping. Here we have used $L=3$. Case (i) should in principle produce the same result as case (ii) if the ω value for case (i) is large enough to reach the asymptotic limit. Figure 3 shows the variation of $R_c/\omega^{3/2}$ with Pr. The variation becomes very steep as Pr becomes small. The dashed curve corresponds to case (i) with $\omega=30$. The solid curve corresponds to case (ii) with the semi-infinite domain formulation. The two curves almost overlap each other. Furthermore, when we compare the result with that from Gershuni and Zhukhovitskii [3], or equivalently with Fig. 4 of Niemela and Donnelly [4], who

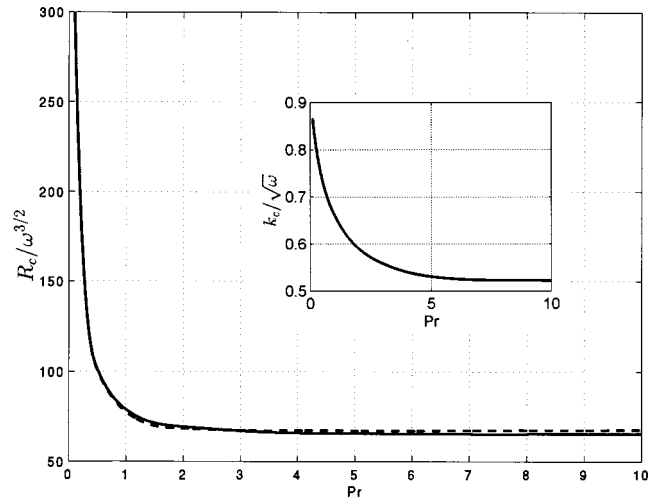


FIG. 3. Comparison $R_c/\omega^{3/2}$ vs Pr for (i) $\omega=900$ (dashed line); (ii) $\omega \rightarrow \infty$. Case (ii) (solid line) uses the semi-infinite domain formulation. The inserted panel shows the overlapping curves of $k_c/\omega^{1/2}$ vs Pr for the cases (i) and (ii).

reproduced the result of Gershuni and Zhukhovitskii, we see that the agreement is reasonably good. Our result shows $R_c/\omega^{3/2} \approx 104$ and 87.2 at $Pr=0.49$ and 0.75 , respectively, compared with the values of 122 and 83 of Niemela and Donnelly [4] at the same Prandtl numbers. The result indicates that $R_c/\omega^{3/2}$ becomes insensitive to Pr when $Pr > 2$. A very similar behavior is observed for the critical wave number, which is shown in the inserted panel, where $k_c/\omega^{1/2}$ is plotted as a function of Pr. In the panel the two wave-number curves for cases (i) and (ii) are indistinguishable.

In Fig. 4, we turn to another comparison. The dashed line connects a set of experimental points obtained from Niemela and Donnelly (private communication) for a fluid with $Pr=0.49$. The solid and dashed-dotted lines connect the points obtained from our numerical computations at the corresponding frequencies with the same value of Pr. The solid and dashed-dotted lines correspond, respectively, to a perfectly conducting and an insulating upper boundary condition. The

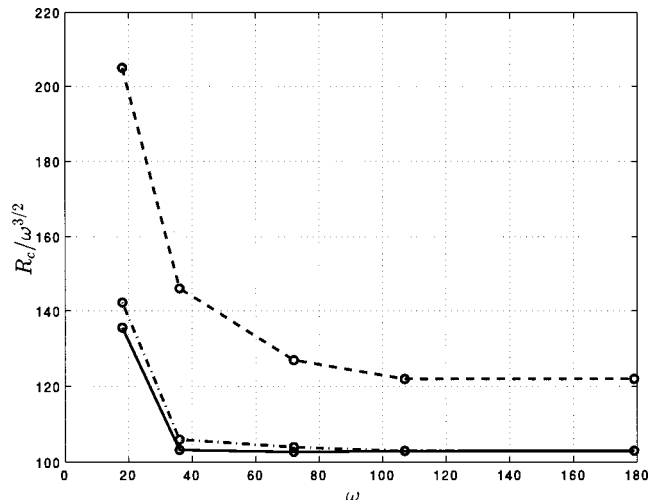


FIG. 4. Comparison of the neutral curve variation in ω obtained by Niemela and Donnelly and by our numerical computations at $Pr=0.49$.

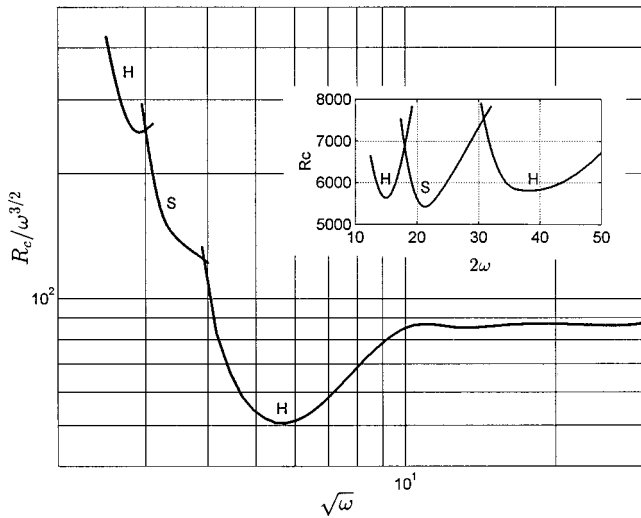


FIG. 5. A log-log plot of $R_c / \omega^{3/2}$ vs $\omega^{1/2}$ for the case of an antisymmetric basic temperature with $Pr=0.73$. Inset: a regular plot of the same quantities to emphasize the alternating neutral curves.

difference arising from the two thermal boundary conditions is small, indicating that the upper wall thermal condition is unimportant for the range of frequencies shown. The difference between the experimental and computational results may be due to side-wall effects in the experiment. But the percentage of disagreement seems to be independent of ω , indicating that another reason is likely.

B. Antisymmetric case

In order to compare with Yih and Li's stability boundaries given in their Fig. 1, we set $Pr=0.73$, the same value as used in their study. The ω defined in Yih and Li's paper corresponds to our 2ω . Only the rightmost H neutral-curve loop in their Fig. 1 has been recalculated here for the purpose of comparison. In our inserted panel to Fig. 5, we plot R_c versus 2ω , the same quantities plotted in Yih and Li's Fig. 1. Our leftmost H neutral-curve loop in the inset corresponds to Yih and Li's rightmost H loop. The difference in the minima

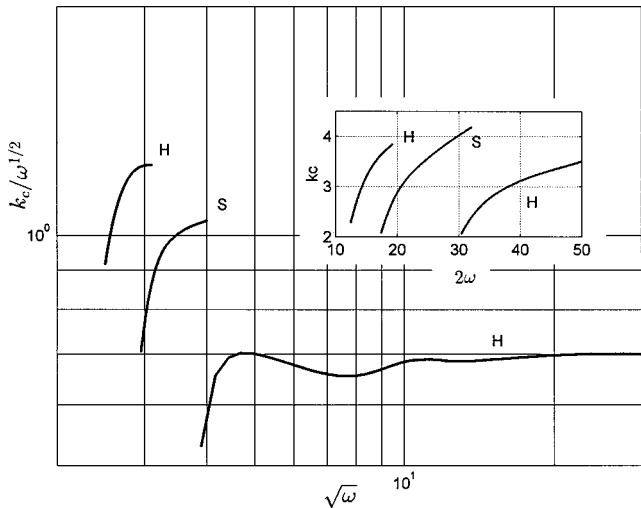


FIG. 6. A corresponding log-log plot of $k_c / \omega^{1/2}$ vs $\omega^{1/2}$ for the antisymmetric case, $Pr=0.73$.

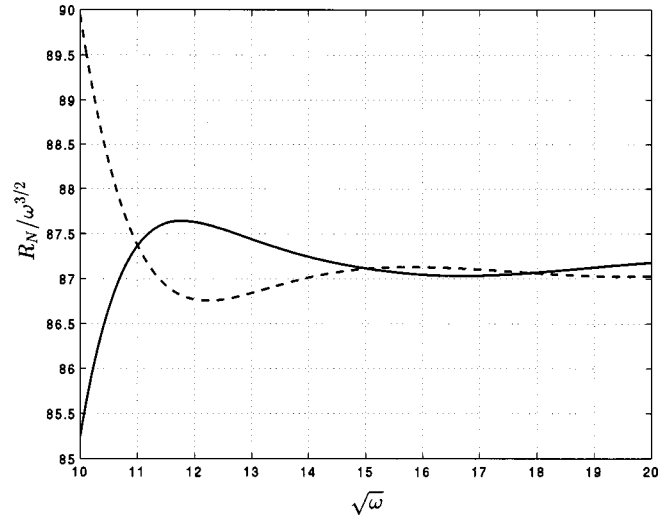


FIG. 7. Plot shows the variation of $R_N / \omega^{3/2}$ for the even mode (solid) and odd mode (dashed) in the antisymmetric case. The wave number is prescribed at $k=0.7\omega^{1/2}$.

of the two curves is within 3%, indicating good agreement. Loops to the left of this H loop are not shown in the present figure. But the low- ω behavior for the antisymmetric case appears to be similar to that of the asymmetric case. In Fig. 1 of Yih and Li, the stability condition for ω below 5 (approximately) is indicated by a number of computed points (corresponding to their leftmost dashed curve) representing the mean positions of the synchronous and subharmonic loops.

Starting with Yih and Li's result corresponding to a H loop at $\omega \approx 18$, we extend their result further to the right. Our results show a S loop following the H loop, and then still another H loop follows. In the log-log plot of Fig. 5, we show $R_c / \omega^{3/2}$ versus $\omega^{1/2}$ for the critical mode of disturbance. The log-log result shows that this last H loop is not followed by another S loop but becomes the asymptotic critical curve for the Stokes layer. Unlike the previous case where the critical curve tends to a constant value in a monotonic fashion, here the neutral curve approaches the asymptotic limit only after first encountering a dip at $\omega^{1/2} \approx 5.6$. Figure 6 shows the corresponding k_c in the inserted panel and the log-log plot of $k_c / \omega^{1/2}$ versus $\omega^{1/2}$. In order to compare the asymptotic values for case (ii) to those for case (i), we set $Pr=7.0$. At $\omega^{1/2}=30$ we obtain $R_c \approx 65.304\omega^{3/2}$ and $k_c \approx 0.525\omega^{1/2}$. The corresponding values for the asymmetric case at $\omega^{1/2}=30$ are $R_c \approx 65.483\omega^{3/2}$ and $k_c \approx 0.525\omega^{1/2}$. The differences for the two cases are insignificant, suggesting that the two boundary layers can be treated independently of each other for $\omega^{1/2} \geq 30$ when $Pr=7.0$.

Since there are two Stokes layers, the disturbance modes can be realized in even or odd symmetry with respect to the midplane when ω is sufficiently large. Their mode shapes will be illustrated in Fig. 8 (see below). The difference in R_c for the even and odd modes is small for high ω . For example, at $\sqrt{\omega}=20$, the R_c for the even and odd modes are, respectively, $87.247\omega^{3/2}$ and $87.031\omega^{3/2}$. The difference is small, suggesting that both modes might have an equal chance of being realizable in experiments at high frequencies. But at a lower frequency, the difference between the two modes can become more pronounced. The results in Fig. 5 are for the even mode. In Fig. 7, we plot the quantity $R_N / \omega^{3/2}$ versus

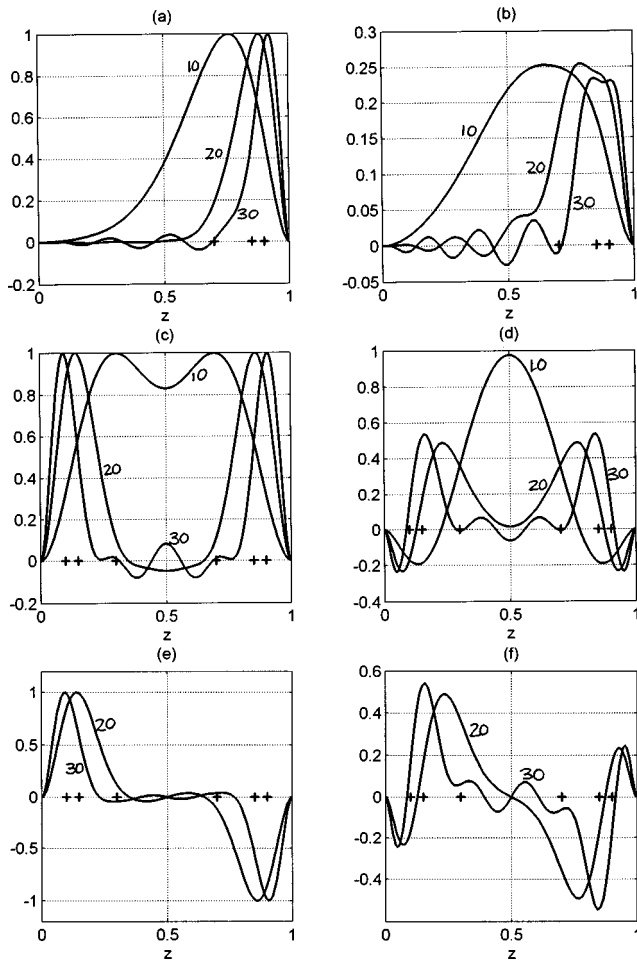


FIG. 8. Vertical dependences of the first two functions in the Fourier expansion corresponding to the $\cos(t)$ term [(a), (c), and (e)], and to the $\sin(t)$ term [(b), (d), and (f)]. Results of $\sqrt{\omega} = 10, 20,$ and 30 show that the disturbances are localized to the boundary layer when ω becomes large.

$\omega^{1/2}$ for neutral instability of the even mode (solid line) and odd mode (dashed line) for the frequency range between $\omega^{1/2} = 10$ and 20 . Since the variation in k_c appears small, we consider the wave number fixed at $0.7\omega^{1/2}$, the critical value for $\omega \approx 20$ and higher. The neutral curves for the even and odd modes intersect three times in the range. For $\omega^{1/2} > 18$, the odd mode is slightly more critical. For $\omega^{1/2} < 11$, the two curves start to diverge from one another and the even mode becomes critical.

In Figs. 8(a)–8(d) we show the z dependence of $\hat{W}_1(z)$ and $\check{W}_1(z)$, which are the first two Fourier coefficients of the cosine and sine components of $W(z, t)$ of the subharmonic solution. Figures 8(a) and 8(b) show the $\hat{W}_1(z)$ and $\check{W}_1(z)$ functions, respectively, for the asymmetric case. Note that there is a pronounced change in the decay of the disturbance outside the Stokes layer, namely, from monotonic to oscillatory decay, as $\omega^{1/2}$ increases from 10 to 30 . The three curves from left to right correspond to $\sqrt{\omega} = 10, 20,$ and 30 . Figures 8(c) and 8(d) show the $\hat{W}_1(z)$ and $\check{W}_1(z)$ functions, respectively, for the antisymmetric case. The three curves from left to right correspond again to the same values of $\sqrt{\omega}$. In Figs. 8(e) and 8(f), we show the even eigenfunctions for the anti-

symmetric case. For a given ω , the maximal disturbance location appears to be shifted slightly towards the interior in comparison with the asymmetric case. In Figs. 8(e) and 8(f) we show $\hat{W}_1(z)$ and $\check{W}_1(z)$ for the odd eigenfunction for the two cases $\sqrt{\omega} = 20$ and 30 . The odd mode is no longer present at $\sqrt{\omega} = 10$.

The value of z at which the maximal amplitude of the disturbance occurs appears to be correlated with the tick marks on the horizontal axis of each panel, which measure the boundary-layer thickness. The correlation is strong as ω becomes larger. In the plots we calibrate the tick marks with the quantity $3/\sqrt{\omega}$, where $1/\sqrt{\omega}$ is proportional to the Stokes layer thickness. A factor 3 is introduced to position these marks roughly at the maxima of the disturbance amplitude for the result of Fig. 8(a). It should be noted, however, that the disturbances penetrate well into the interior of the layer as well.

IV. DISCUSSION

In most of the studies of modulated thermal convection done so far, the modulation occurs about a state with a non-zero mean temperature gradient, i.e., the effects of modulation upon classical Rayleigh-Bénard convection have been studied. Upon the use of Floquet theory for the linearized equations, the classical linear critical value of $R_c \approx 1707.76$ without modulation has been shown to increase with modulation but it has also been shown that the shift becomes small as ω becomes large for moderate amplitudes of modulation [15]. However, it is now clear that, at high frequencies and large modulation amplitudes, a second instability associated with the thermal Stokes layer can occur. It is therefore of interest to estimate the range of mean ΔT^* for which the present analysis describes adequately the instability of the thermal Stokes layer when a mean gradient of temperature is present. Conversely, it is important to state the conditions under which the instability of the thermal Stokes layer can be ignored if one is primarily interested in estimating the effects of modulation upon conventional Rayleigh-Bénard convection based on the results of earlier studies.

The mean and oscillating effects are characterized by two nondimensional parameters,

$$R_{\Delta T^*} = \frac{\alpha g \Delta T^* d^3}{\nu \kappa}, \quad R_{T_\delta^*} = \frac{\alpha g T_\delta^* d^3}{\nu \kappa}, \quad (15)$$

which are the Rayleigh numbers measuring the mean temperature difference and the oscillating wall temperature, respectively. From the foregoing results, an asymptotic relationship $R_{T_\delta^*} = a \omega^{3/2}$ is obtained roughly for $\omega^{1/2} > 10$, where “ a ” is a constant for a given fluid. For a layer which is unstable to Rayleigh-Bénard convection at a certain temperature difference ΔT^* , a moderate magnitude of T_δ^* typically exerts a stabilizing effect. But as T_δ^* increases, there is a point where the layer becomes unstable solely due to T_δ^* . This value of T_δ^* can be estimated as follows:

$$\frac{T_\delta^*}{\Delta T^*} = \frac{R_{T_\delta^*}}{R_{\Delta T^*}} \sim \frac{a}{1707.76} \omega^{3/2}.$$

Now, a depends on Pr . But according to the result of Fig. 3, a becomes insensitive to the change of Pr for $Pr > 2$. We take this value of a equal to 80.4 (see the results in Sec. III A) and estimate that

$$\frac{T_{\delta}^*}{\Delta T^*} = 0.0471 \omega^{3/2}.$$

If ω is large, say $\omega = 10^2$, we obtain $T_{\delta}^* \approx 47.1 \Delta T^*$. In other words, the oscillating temperature must be more than 50 times the mean temperature difference if the latter is to have an insignificant effect.

V. CONCLUSION

The problem of the onset of convection in a fluid layer when the temperatures of one or both walls vary periodically with time about a reference temperature has been studied numerically in this paper for more general values of the non-dimensional frequency parameter ω than done previously. For the case of asymmetric modulation of one wall, it is shown that the alternating sequence of synchronous and subharmonic instabilities characteristic of the low-frequency regime disappears when $\omega^{1/2}$ reaches a value of 1.9 approxi-

mately. For $\omega^{1/2} > 1.9$, the critical disturbance corresponds to only a subharmonic solution. For the case with antisymmetric modulation, there are two localized disturbances, each of which is associated with a Stokes layer at the wall. Both even and odd critical modes can exist for the antisymmetric case at sufficiently large ω . For $\omega^{1/2} \sim O(1)$, our recalculation agrees reasonably well with Yih and Li's. The layer is more unstable to the antisymmetric than the asymmetric modulation. There appear to be interactions between the two unstable Stokes layers for ω as large as 9×10^2 via penetration of the disturbance outside the Stokes layers. It would naturally be of interest to explore the weakly nonlinear problem in order to get a better idea of the role of the subcritical instability discussed by Swift and Hohenberg [5] over a wider range of ω . We hope to pursue this aspect in another paper.

ACKNOWLEDGMENTS

This research has been supported by the NASA Microgravity Fluid Physics Program through Grant No. NAG3-1819. The authors would like to express their gratitude to J. J. Niemela and R. D. Donnelly for the additional data from their experiment.

-
- [1] C. W. Meyer, D. S. Cannell, and G. Ahlers, *Phys. Rev. A* **45**, 8583 (1992).
 - [2] G. Z. Gershuni and E. M. Zhukhovitskii, *Prikl. Mekh. Tekh. Fiz.* **6**, 55 (1965).
 - [3] G. Z. Gershuni and E. M. Zhukhovitskii, *Convective Instability of Incompressible Fluids* (Keter, Jerusalem, 1976).
 - [4] J. J. Niemela and R. J. Donnelly, *Phys. Rev. Lett.* **57**, 583 (1986).
 - [5] J. B. Swift and P. C. Hohenberg, *Phys. Rev. A* **36**, 4870 (1987).
 - [6] C. S. Yih and C. H. Li, *J. Fluid Mech.* **54**, 143 (1972).
 - [7] K. Kumar, *Proc. R. Soc. London, Ser. A* **452**, 1113 (1996).
 - [8] E. Cerda and E. Tirapegui, *Phys. Rev. Lett.* **78**, 859 (1997).
 - [9] E. A. Cerda and E. L. Tirapegui, *J. Fluid Mech.* **368**, 195 (1998).
 - [10] A. C. Or, *J. Fluid Mech.* **335**, 213 (1997).
 - [11] C. F. Barengi and C. A. Jones, *J. Fluid Mech.* **208**, 127 (1989).
 - [12] J. Dowden, *J. Fluid Mech.* **110**, 149 (1981).
 - [13] A. C. Or (unpublished).
 - [14] C. Canuto, M. Y. Hussaini, A. Quarteroni, and T. A. Zang, *Spectral Methods in Fluid Dynamics* (Springer-Verlag, New York, 1986).
 - [15] S. H. Davis, *Annu. Rev. Fluid Mech.* **8**, 57 (1976).